NASA/CR-2002-211661
ICASE Report No. 2002-21

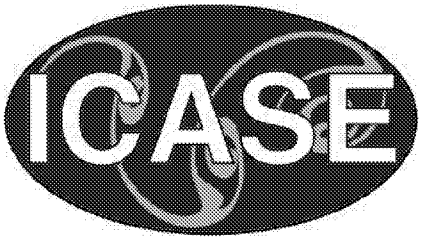

Lateral Migration and Rotational Motion of Elliptic Particles in Planar Poiseuille Flow

Dewei Qi
Western Michigan University, Kalamazoo, Michigan

Li-Shi Luo
ICASE, Hampton, Virginia

Raja Aravamuthan
Western Michigan University, Kalamazoo, Michigan

William Strieder
University of Notre Dame, Notre Dame, Indiana

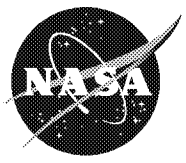

July 2002

The NASA STI Program Office . . . in Profile

Since its founding, NASA has been dedicated to the advancement of aeronautics and space science. The NASA Scientific and Technical Information (STI) Program Office plays a key part in helping NASA maintain this important role.

The NASA STI Program Office is operated by Langley Research Center, the lead center for NASA's scientific and technical information. The NASA STI Program Office provides access to the NASA STI Database, the largest collection of aeronautical and space science STI in the world. The Program Office is also NASA's institutional mechanism for disseminating the results of its research and development activities. These results are published by NASA in the NASA STI Report Series, which includes the following report types:

- TECHNICAL PUBLICATION. Reports of completed research or a major significant phase of research that present the results of NASA programs and include extensive data or theoretical analysis. Includes compilations of significant scientific and technical data and information deemed to be of continuing reference value. NASA's counterpart of peer-reviewed formal professional papers, but having less stringent limitations on manuscript length and extent of graphic presentations.

- TECHNICAL MEMORANDUM. Scientific and technical findings that are preliminary or of specialized interest, e.g., quick release reports, working papers, and bibliographies that contain minimal annotation. Does not contain extensive analysis.

- CONTRACTOR REPORT. Scientific and technical findings by NASA-sponsored contractors and grantees.

- CONFERENCE PUBLICATIONS. Collected papers from scientific and technical conferences, symposia, seminars, or other meetings sponsored or cosponsored by NASA.

- SPECIAL PUBLICATION. Scientific, technical, or historical information from NASA programs, projects, and missions, often concerned with subjects having substantial public interest.

- TECHNICAL TRANSLATION. English-language translations of foreign scientific and technical material pertinent to NASA's mission.

Specialized services that complement the STI Program Office's diverse offerings include creating custom thesauri, building customized data bases, organizing and publishing research results . . . even providing videos.

For more information about the NASA STI Program Office, see the following:

- Access the NASA STI Program Home Page at ***http://www.sti.nasa.gov***

- Email your question via the Internet to help@sti.nasa.gov

- Fax your question to the NASA STI Help Desk at (301) 621-0134

- Telephone the NASA STI Help Desk at (301) 621-0390

- Write to:
  NASA STI Help Desk
  NASA Center for AeroSpace Information
  7121 Standard Drive
  Hanover, MD 21076-1320

NASA/CR-2002-211661
ICASE Report No. 2002-21

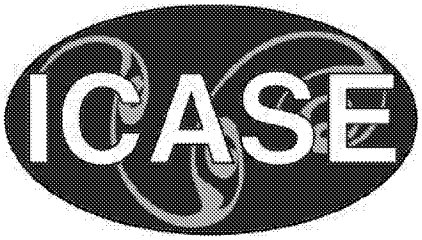

Lateral Migration and Rotational Motion of Elliptic Particles in Planar Poiseuille Flow

Dewei Qi
Western Michigan University, Kalamazoo, Michigan

Li-Shi Luo
ICASE, Hampton, Virginia

Raja Aravamuthan
Western Michigan University, Kalamazoo, Michigan

William Strieder
University of Notre Dame, Notre Dame, Indiana

ICASE, NASA Langley Research Center
Hampton, Virginia
Operated by Universities Space Research Association

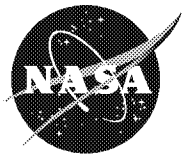

Prepared for Langley Research Center
under Contract NAS1-97046

July 2002

Available from the following:

NASA Center for AeroSpace Information (CASI)
7121 Standard Drive
Hanover, MD 21076-1320
(301) 621-0390

National Technical Information Service (NTIS)
5285 Port Royal Road
Springfield, VA 22161-2171
(703) 487-4650

LATERAL MIGRATION AND ROTATIONAL MOTION OF ELLIPTIC PARTICLES IN PLANAR POISEUILLE FLOW

DEWEI QI*, LI-SHI LUO†, RAJA ARAVAMUTHAN‡, AND WILLIAM STRIEDER§

Abstract. Simulations of elliptic particulate suspensions in the planar Poiseuille flow are performed by using the lattice Boltzmann equation. Effects of the multi-particle interaction on the lateral migration and rotational motion of both neutrally and non-neutrally buoyant elliptic particles are investigated. Low and intermediate total particle volume fraction $f_a = 13\%$, 25%, and 40% are considered in this work.

Key words. elliptic particulate suspensions in the planar Poiseuille flow, lateral migration, rotational motion, multi-particle interaction, the Segré and Silberberg effect, lattice Boltzmann simulation

Subject classification. Fluid Mechanics

1. Introduction. Particle suspensions in pressure driven flows can be found in many industrial applications such as transport and refining petroleum, paper manufacturing, pharmaceutical processing and environmental waste treatment. An understanding of the detailed dynamical behavior of particulate suspensions in pressure driven flows (lateral migration, rotational motion, and spatial distribution of particles) would aid designing and developing feasible and economic industrial processes. For many years the research activity in this area has been focused on the investigation of the dynamic behavior of suspensions in the Poiseuille flow.

Segré and Silberberg [25, 26] found that a neutrally buoyant particle migrates to an equilibrium position between a channel wall and the channel centerline due to the wall effect, the velocity profile curvature and shear force. This phenomenon, attributed to the nonlinear inertia effect, has been confirmed in both theory and experiments [3, 4, 16, 8], and more recently in direct numerical simulations [6, 7, 10, 11].

Feng, Hu and Joseph [6, 7] have simulated the motion of a single circular particle in the planar Poiseuille flow by using a finite element method. Both neutrally and non-neutrally buoyant particles were examined. For a neutrally buoyant particle, the Segré-Silberberg phenomenon was reproduced in the simulations and it was found that the equilibrium position is closer to the wall at a higher flow velocity. For a non-neutrally buoyant particle, when the density difference between the particle and the fluid is small, the equilibrium position is either close to the wall or to the centerline, depending on whether the particle leads ahead or lags behind the fluid velocity locally. When the density difference (or the buoyancy effect) is large enough, the particle always moves to the centerline regardless whether it is lighter or heavier than the fluid. In general, a difference in the relative velocity across a solid particle may drive the particle to move laterally since the side with a higher relative velocity may experience a lower pressure. Therefore, these authors suggested four mechanisms responsible for the particle motion in the Poiseuille flow: (1) wall lubrication repulsion, (2) inertial lift due to shear slip, (3) a lift due to particle rotation, and (4) a lift associated with the curvature of the undisturbed velocity profile.

*Department of Paper and Printing Science and Engineering, Western Michigan University, Kalamazoo, MI 49008.

†ICASE, Mail Stop 132C, NASA Langley Research Center, 3 West Reid Street, Building 1152, Hampton, VA 23681-2199 (email address: luo@icase.edu). This research was supported by the National Aeronautics and Space Administration under NASA Contract No. NAS1-97046 while the author was in residence at ICASE, NASA Langley Research Center, Hampton, VA 23681-2199.

‡Department of Paper and Printing Science and Engineering, Western Michigan University, Kalamazoo, MI 49008.

§Department of Chemical Engineering, University of Notre Dame, Notre Dame, IN 46556.

Little information on the motion of elliptic particle in a pressure driven flow is available in literature. In the present paper, we report the direct numerical simulation results for the systems of a single elliptic particle or multiple elliptic particles in the planar Poiseuille flow by using the lattice Boltzmann (LB) method. Both neutrally and non-neutrally buoyant particles are investigated. Only low and intermediate values of the total particle volume (area) fraction, *i.e.* $f_a = 13\%$, 25%, and 40% are considered in the simulations. Effects of the multi-particle interaction on the migration and rotational motion of particles are also analyzed.

2. Theory and simulation method. The fluid flow is governed by the Navier Stokes equations:

$$\rho_f \partial_t \mathbf{u} + \rho_f \mathbf{u} \nabla \mathbf{u} = -\nabla P + \eta \nabla^2 \mathbf{u} + \rho_f \mathbf{g} \tag{2.1}$$

where ρ_f, $\mathbf{u}$, P, η, and $\mathbf{g}$ are the fluid density, the velocity field, the pressure field, the fluid viscosity, and the acceleration due to gravity, respectively. The equations of motion for the solid particle are

$$m\frac{d\mathbf{U}}{dt} = m\mathbf{g} + \mathbf{F}, \tag{2.2a}$$

$$\mathsf{I} \cdot \frac{d\mathbf{\Omega}}{dt} = \mathbf{T}, \tag{2.2b}$$

where m, $\mathbf{U}$, $\mathbf{\Omega}$, I, are the mass, the linear velocity, the angular velocity, and the moment of inertia tensor of the particle, respectively; $\mathbf{F}$ and $\mathbf{T}$ are the hydrodynamic force and torque exerted on the particle, respectively.

The Navier-Stokes equations can be simulated by the lattice Boltzmann equation (LBE) [27, 5, 18, 17, 9, 14, 15, 13, 1, 2]. The motion of nonspherical particles can be handled by solving the equations of motion for each particle [19, 20, 21]. In the past, the LBE method has been successfully used to simulate two-dimensional (2D) rectangular particles and three-dimensional (3D) beds of cylinders in sedimentation flows [22, 23]. In these simulations, the numerical results agree with experimental data very well and the direct numerical simulations by using the LBE method have quantitatively captured the essential physics of the particle-fluid-flow, and thus can be able to correctly predict the flow phenomena. Therefore, the same method is used in this work. The details of the LBE method has been reported elsewhere (cf. [14, 15, 2, 21]) and will not be repeated here. In the present work, it is assumed that when two particles collide, an elastic collision occurs. In other words, the linear and angular momenta of each particle are conserved during the collision. This hard shell scheme, developed by Rebertus and Sando [24] for molecular dynamic simulations and adopted by Qi [22, 23] for sedimenting cylinders, will be used in this work.

3. Simulations and Results. One can find that the Poiseuille flow is determined by four dimensionless parameters [12]

$$\rho_s = \frac{\rho_p}{\rho_f}, \qquad C = \frac{2a}{W}, \qquad \mathrm{Re} = \frac{4a^2\rho_f\gamma}{\eta}, \qquad G = \frac{2a(\rho_p - \rho_f)g}{\gamma\eta}, \tag{3.1}$$

where ρ_s is the ratio of solid density ρ_p to fluid density ρ_f, W is the width of the channel, a is the radius of the principal axis of the elliptic particle, C is the confinement ratio, γ is the local shear rate of flow, and Re is the particle Reynolds number. In the planar Poiseuille flow, the shear rate

$$\gamma = \frac{4U_m}{W}\left(1 - \frac{2x}{W}\right)$$

is not a constant and varies with coordinate x in the cross flow direction, where U_m is the maximum velocity of the undisturbed flow in the channel. We use the shear rate at $x = W/4$ to estimate the particle Reynolds

number unless otherwise stated in this work, *i.e.*,

$$\mathrm{Re} = \frac{8a^2 U_m}{\nu W},$$

where ν is the kinematic viscosity of the fluid. The dimensionless parameter

$$S = \frac{\mathrm{Re}}{G} = \frac{2a\gamma^2}{\left(\frac{\rho_p}{\rho_f} - 1\right) g} \tag{3.2}$$

measures the ratio of life to buoyant weight, which will be used later.

In the simulation presented here, a constant body force simulating the gravity is used to achieve the effect of constant pressure gradient in the Poiseuille flow. The flow and gravity are along the y-direction, as shown in Fig. 1. And the periodic boundary conditions are applied in the y-direction, as shown in Fig. 1. The bounce-back boundary conditions are applied at walls as well as the surface of particles to mimic the noslip boundary conditions. The bounce-back scheme used here for the fluid-solid interface of a moving particle is first proposed by Ladd [14], improved by Aidun *et al.* [2], and is discussed in detail in [21].

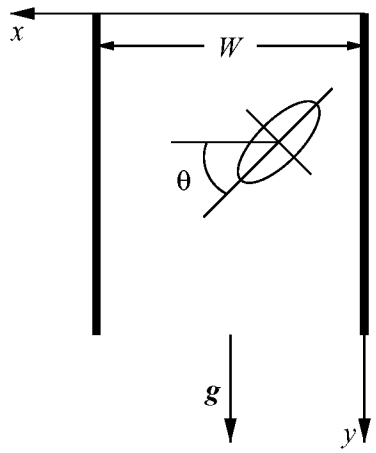

FIG. 1. *The planar Poiseuille flow configuration. Gravity and flow are in the y-direction (down).*

3.1. Neutrally buoyant elliptic single particle. Before investigating a multi-particle system, the migration of a singe elliptic particle is studied first. A computational domain of size 251×251 in lattice unit is used. The major radius of the ellipse is $a = 15$ and the minor radius is $b = 7.5$. The confinement ratio $C = 0.12$ for all the cases. The bulk Reynolds number of suspension is defined by

$$\mathrm{Re}_b = \frac{W V_a}{\nu},$$

where V_a is the average velocity of the suspension and ν is the kinematic viscosity.

First, four simulations of a single neutrally buoyant elliptic particle with different initial positions in the x-direction (the cross flow direction) are performed at $\mathrm{Re}_b = 140.625$. In each of the four runs, the elliptic particle migrates to the equilibrium position approximately $0.156W$ away from a wall. This equilibrium position is independent of the initial orientation and position, as shown in Fig. 2. However, it takes a much longer time for a particle with an initial position close to the center of channel to reach the equilibrium position because the shear rate at the channel center is zero. The Segré-Silberberg phenomenon is observed

in the system of a neutrally buoyant elliptic particle in the planar Poiseuille flow. The results show that the particle always lags behind the flow locally and the effect of velocity curvature indeed pushes the particle toward the wall. This mechanism has been clearly explained by Feng, Hu, and Joseph [7].

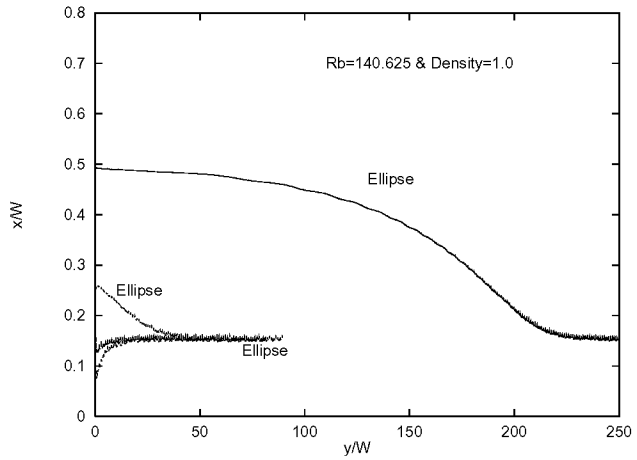

FIG. 2. *The migration of a neutrally buoyant elliptic particle with different initial positions x_0. There are four simulations for single ellipse at $Re_p = 140.625$. All distances are normalized by the width of channel W. The same is applied to other figures. The wiggles are caused by the discrete effect of the solid particle.*

The ellipse always rotates at its equilibrium state because the particle still experiences a shear force. The angular velocity is periodic in time. The rotational rate at the final equilibrium state is plotted in Fig. 3 for the neutrally buoyant particle.

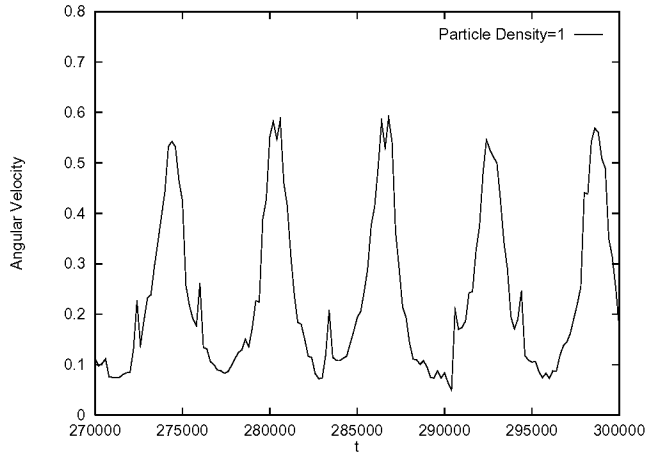

FIG. 3. *The angular velocity as a function of time for a neutrally buoyant particle.*

In order to describe the orientation of the particle, an averaged angular distribution across the channel is used:

$$f(\theta) = \langle \delta(\theta - \theta(t)) \rangle_t \,, \tag{3.3}$$

where δ is a Dirac function, and $\langle \cdot \rangle_t$ is the average performed over an ensemble of trajectories $\theta(t)$ at a given position x. The averaged angular distribution $f(\theta)$ gives the probability of ellipse along angle θ. The angular distribution function is normalized to unity over the interval of $[0, \pi]$. Fig. 4 shows that the ellipse is

much more likely to align its long axis with the flow direction (y-direction) because the particle experiences a weaker torque from the flow when it is in alignment with the flow.

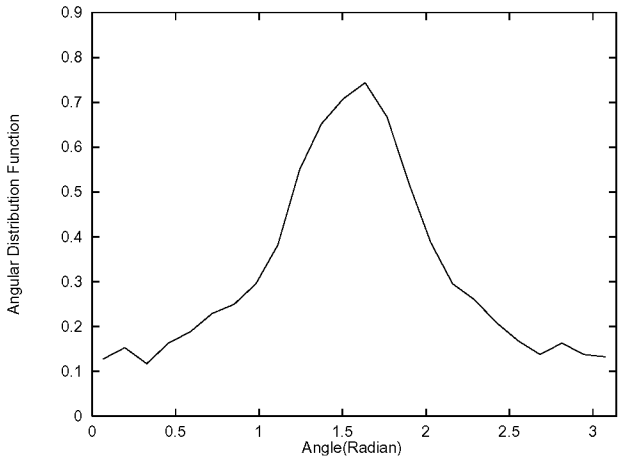

FIG. 4. *The angular distribution function of neutrally buoyant particle.*

3.2. Non-neutrally buoyant single particle. When the particle density is slightly larger than fluid density ($\rho_s = 1.005$, Re $= 6.08$, and $G = 27.7$), the particle leads the flow velocity locally and the relative velocity at the side of the particle closer to the wall is increased, resulting in a lower pressure due to a higher relative velocity on this side. The particle migrates to a wall due to the pressure difference and stabilizes at a position closer to a wall than does a neutrally buoyant particle. In this case the ratio of the lift to buoyant weight $S = 0.22$.

When the solid density is sufficiently larger than the fluid density ($\rho_s = 1.01$, Re $= 6.08$, and $G = 55.4$), the particle motion resembles that of sedimentation. The wall repulsion overpowers the inertial lift and the velocity curvature effect, and the particle moves to the centerline. Figure 5 shows the migrations for the cases of $\rho_s = 1.005$ and $\rho_s = 1.01$. For the purpose of comparison, the migration for a neutrally buoyant ellipse ($\rho_s = 1$) is also shown in the same figure. It is clear that sedimentation is the major force driving the particles from the wall to the channel center when the density of ellipse is large enough (*e.g.*, $\rho_s = 1.01$). This can be seen more clearly from the averaged angular distribution across the channel. In a sedimentation flow, the orientation of an ellipse along the cross flow direction is dominant due to the wakes associated with the nonlinear inertia effect. The angle θ (cf. Fig. 1) of the ellipse as a function of time is depicted in Fig. 6 for the cases of $\rho_s = 1.005$ and $\rho_s = 1.01$. The ellipse of $\rho_s = 1.01$ turns quickly to the horizontal direction or the cross flow direction around $\theta = 0°$, while the ellipse of $\rho_s = 1.005$ turns to the flow direction or vertical direction, oscillating approximately around $\theta = 83°$. It is evident that when $\rho_s = 1.01$ the sedimentation effect is dominant since the long end of the particle turns to the horizontal direction and the particle moves to the centerline ($x/W = 1/2$), where the shear rate vanishes. In contrast, the particle with $\rho_s = 1.005$ turns to the vertical direction and moves toward to the wall. This behavior may be attributed to the combined effects of the Poiseuille flow and sedimentation. The shear lift and the wall effect force the particle to orient in the vertical direction. Huang, Hu and Joseph [11] pointed out that the particle may turn to the vertical direction due to the wall effect at a small particle Reynolds number in a sedimentation flow. Similarly, the wall effect also contributes to the determination of the particle orientation when $\rho_s = 1.005$. In these two cases, the particle ceases to rotate due to the sedimentation and the wall effect. However, the rotational behavior of a neutrally buoyant ellipse is entirely different from that of the above two buoyant cases of $\rho_s > 1$.

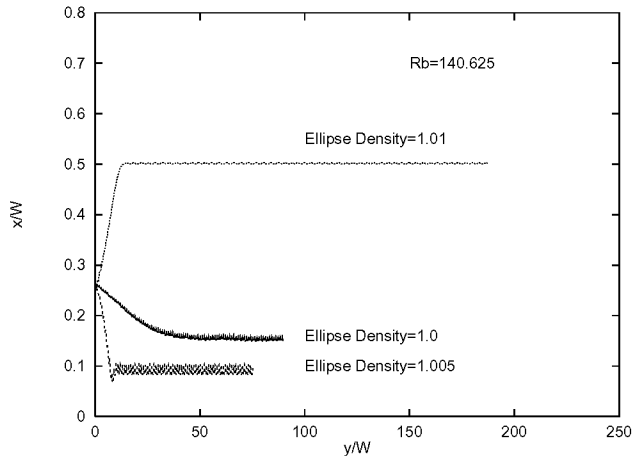

FIG. 5. *The migration of ellipse with* $\rho_s = 1.0$, 1.005 *and* 1.01 *at* $\mathrm{Re}_b = 140.625$. *The wiggles are due to the discrete effect in the particle-fluid interfaces.*

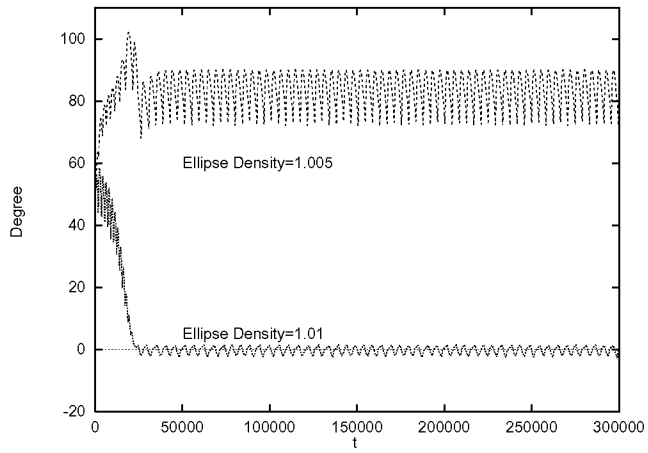

FIG. 6. *The rotational angles of ellipse as a function of time for the cases of* $\rho_s = 1.005$ *and* 1.01 *at* $\mathrm{Re}_b = 140.625$.

The neutrally buoyant particle is always rotating, and is much more likely to align its long axis with the flow direction than with the cross flow direction, as previously discussed and shown in Fig. 4.

As previously mentioned, the neutrally buoyant particle lags slightly behind the local velocity of the undisturbed flow and the particle moves toward the wall. When the particle is slightly lighter than the fluid ($\rho_s = 0.9995$, $\mathrm{Re} = 6.08$, $G = -2.77$), the lagging velocity increases. The relative velocity at the end of the particle closer to a wall (cf. Fig. 1) becomes larger, and the inertial lift pushes the particle to the centerline. At an even lighter particle density ($\rho_s = 0.995$, $\mathrm{Re} = 6.08$, $G = -27.7$), the lagging velocity further increases, and a stronger wall repulsion forces the particle to move across the centerline, where the particle experiences the same repulsive forces in opposite direction by symmetry of the flow. Therefore, the particle swings back and forth, oscillating about the centerline as shown in Fig. 7. Again, when the sedimentation effect is dominant for the particle of $\rho_s = 0.995$, the particle ceases to rotate on average in time. Whereas for the particle with less buoyancy ($\rho_s = 0.9995$), it never stops rotating, because the sedimentation effect is not dominant in this case.

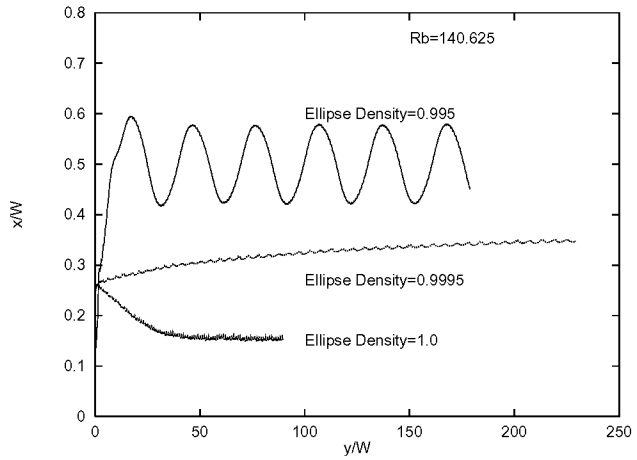

FIG. 7. *The migration of ellipse with* $\rho_s = 1.0$, 0.995, *and* 0.9995 *at* $\mathrm{Re}_b = 140.625$.

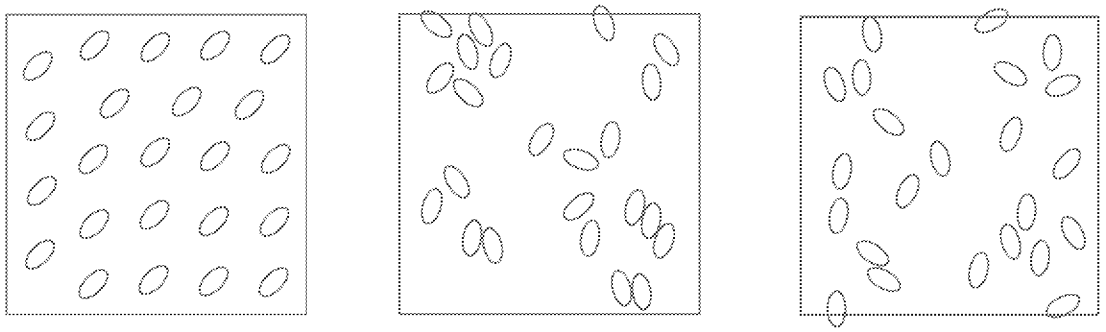

FIG. 8. *The snap shots of the particle configurations of 23 neutrally buoyant elliptic particles with the volume fraction* $f_a = 13\%$ *at time steps (from left to right)* $t = 0$, 300,000, *and* 400,000.

3.3. Neutrally buoyant multi-particles. To study the multi-particle interaction, the motion of 23 neutrally buoyant elliptic particles in the Poiseuille flow is simulated with the same computational domain. In this case, the particle volume (area) fraction f_a is 13%, and the bulk Reynolds number is 140.625. Three snap shots of the particle configurations at $t = 0$, 300,000, and 400,000 are shown in Fig. 8. It is clearly seen that the particles move to the positions between the walls and the centerline. There are two maxima in the averaged volume fraction distribution across the channel and these maxima are located between the walls and centerline, as shown in Fig. 9. However, the maxima are closer to the centerline for the multi-particle system than for the single particle system because multi-particle interaction reduces the curvature effect of the flow. It seems that the particles form clusters, as shown in Fig. 8. With a careful observation, it is found that there are two small shoulders at the averaged velocity distribution across the channel shown in Fig. 10. The locations of the shoulders on the velocity distribution correspond to the maxima of the volume fraction distribution across the channel, indicating that the averaged velocity of particles is suppressed at areas of higher particle volume fraction f_a. This is expected because higher effective viscosity due to higher particle volume fraction reduces the velocity gradient in these areas.

Next, the averaged multi-particle angular distribution function is used to describe the orientation of

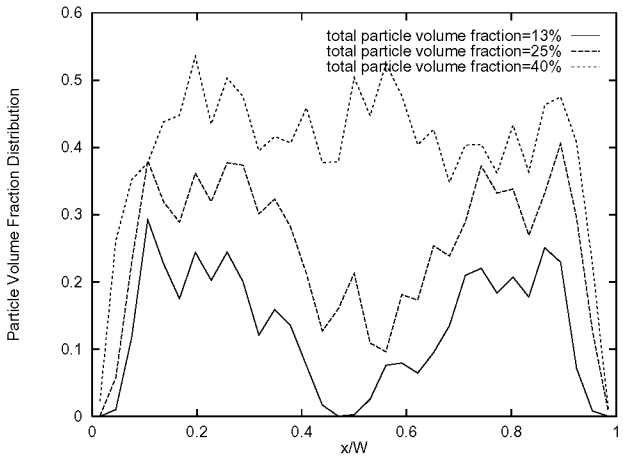

FIG. 9. *The particle volume fraction distribution across the channel for neutrally buoyant particles* ($\rho_s = 1.0$) *at* $f_a = 13\%$, 25%, *and* 40%.

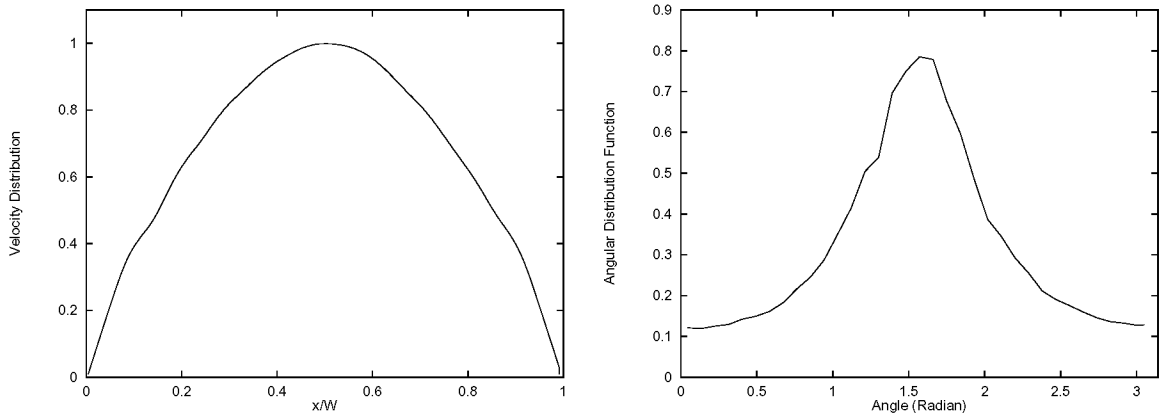

FIG. 10. *Twenty-three neutrally buoyant ellipses* ($\rho_s = 1$) *at* $f_a = 13\%$. (*left*) *The velocity distribution, and* (*right*) *the angular distribution function.*

multi-ellipses:

$$f(\theta) = \frac{1}{N} \sum_{i=1}^{N} \langle \delta(\theta - \theta_i) \rangle_{\theta_i} ,$$

where N is the total number of particles and i indicates the i-th particle. The results in Fig. 10 show that the neutrally buoyant elliptic particles have a much higher probability to align in the flow direction than in the cross flow direction.

To investigate the effect of the total particle volume fraction f_a on migration, the simulations of 44 and 70 elliptic particles are conducted, corresponding to $f_a = 25\%$ and 40%; and $\mathrm{Re}_b = 71.81$ and 75.78, respectively. The results show that the maxima of the average particle volume fraction distribution across the channel become broader and the minimum gradually disappears as the total particle volume fraction f_a increases (Fig. 9). It is observed that the rotational motion of an individual particle is also suppressed by the interactions from its neighboring particles. Thus, the lift due to rotation is reduced and particles may move more closely to the centerline. The velocity distribution of flow becomes flatter (cf. Fig. 11). These results suggest that the Segré-Silberberg effect becomes weaker due to multi-particle interaction, as the total

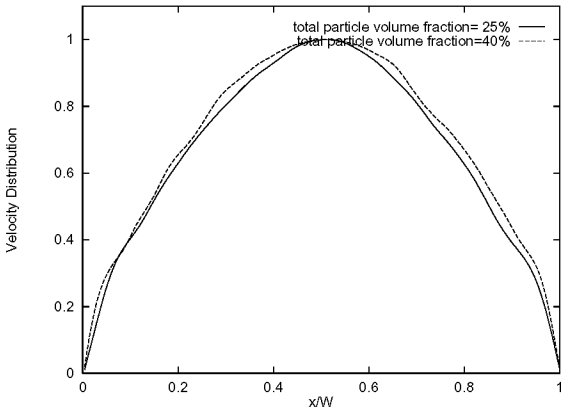

FIG. 11. *The velocity distributions of neutrally buoyant multi-particles at* $f_a = 25\%$ *and* $f_a = 40\%$. *The velocity is normalized by the maximum velocity.*

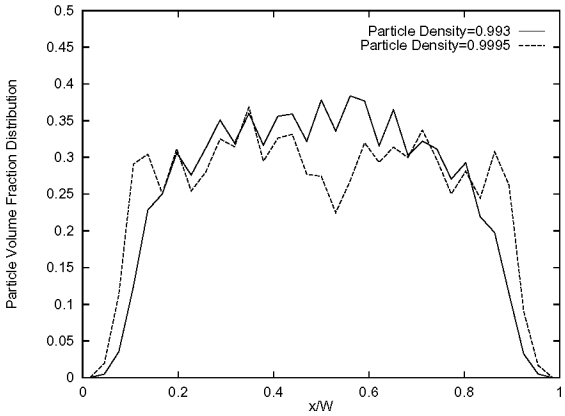

FIG. 12. *The averaged volume fraction distribution across the channel for elliptic particles with the densities of* $\rho_s = 0.993$ *and* $Re_b = 109.38$, *and of* $\rho_s = 0.9995$ *at* $Re_b = 129.7$. *The total particle volume fraction for the two systems is* $f_a = 25\%$

particle volume fraction increases.

3.4. Non-neutrally buoyant multi-particles. When the particle density is slightly lighter than the fluid density (*e.g.*, $\rho_s = 0.9995$), the two maxima between the walls and the centerline on the averaged particle volume fraction distribution across the channel become much wider, as shown in Fig. 12, compared to that of the neutrally buoyant particles (Fig. 9). As the particle density further decreases to $\rho_s = 0.993$, the two maxima finally merge together, thus the volume fraction distribution across the channel now has only one wide maximum around the centerline as shown in Fig. 12. The two shoulders on the curve of velocity profile become more prominent and the velocity profile becomes flat. The probability of ellipses aligning with the flow is also greatly reduced, as shown in Fig. 13.

Finally, the system of 44 buoyant elliptic particles ($f_a = 25\%$) with $\rho_s = 1.002$ and $\rho_s = 1.015$ are studied and compared with the system of 44 neutrally buoyant particles ($\rho_s = 1.0$). When particles are slightly heavier than the fluid ($\rho_s = 1.002$), they move to the region closer to the walls than do the neutrally buoyant particles due to the inertial lift forces. In this case, the behavior of the multi-particle system is similar to that of a single particle. As shown in Fig. 15, the maxima of the averaged volume fraction distribution across the channel are located more closely to both walls for slightly heavier particles ($\rho_s = 1.002$) than for

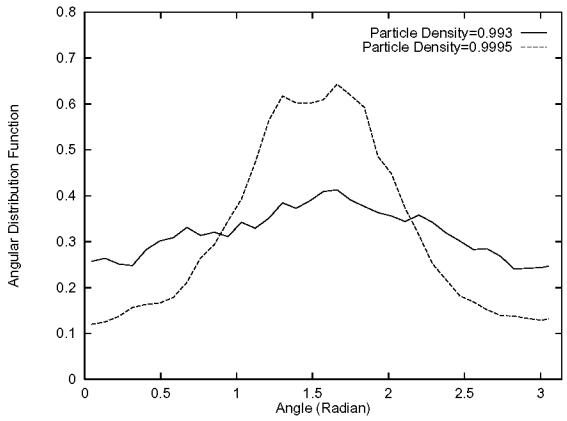

FIG. 13. *The angular distribution functions for the same cases as in Fig. 12.*

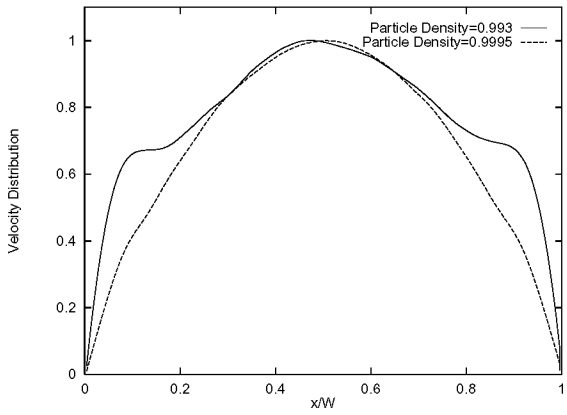

FIG. 14. *The velocity distributions for the same cases as in Fig. 12.*

neutrally buoyant particles. As the particle density increases to $\rho_s = 1.015$, more particles move from the wall regions to the central region. By comparing the angular distribution functions of the neutrally buoyant particles and the heaviest particles ($\rho_s = 1.015$) in Fig. 16, it can be seen that when $\rho_s = 1.015$ the likelihood of particles aligning with the flow is greatly reduced by sedimentation, which turns ellipses from the flow direction to the cross flow direction.

The inertial lift associated with the curvature effect in this case still exists, although it is relatively weak. Therefore, the averaged particle volume fraction distribution across the channel, the angular distribution function, and the velocity distribution, respectively shown in Fig. 15, 16, and 17, demonstrate the combined effects of the Poiseuille flow and sedimentation. It is clearly shown in Fig. 17 that the velocity profile for the heavier buoyant particles of $\rho_s = 1.015$ is broader than that for the lighter buoyant particles of $\rho_s = 1.002$, and the velocity profile for the lighter buoyant particles of $\rho_s = 1.002$ is broader than that for the neutrally buoyant particles.

4. Conclusions. The lattice Boltzmann method has been employed to simulate the dynamic migration and rotational behavior of a single elliptic particle and multiple elliptic particles in the planar Poiseuille flow. The buoyancy effect on the lateral migration of the particles is analyzed. The total particle volume fractions of 13%, 25% and 40%, are considered in the simulations. Several conclusions can be drawn from this work.

First of all, for the system consisting of a single neutrally buoyant elliptic particle or multiple particles,

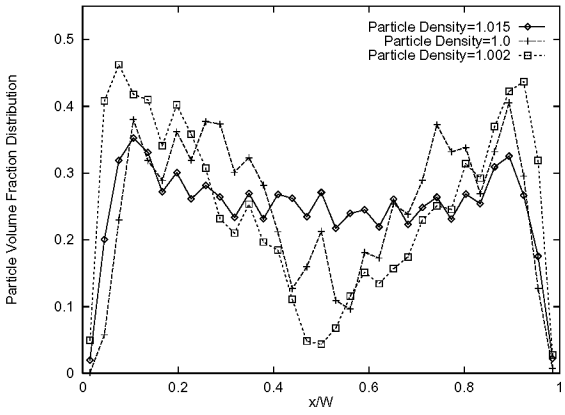

FIG. 15. *The averaged particle volume fraction distributions for elliptic particles with the density of* $\rho_s = 1.0$ *at* $\mathrm{Re}_b = 75.78$, *of* $\rho_s = 1.002$ *at* $\mathrm{Re}_b = 82.81$ *and of* $\rho_s = 1.015$ *at* $\mathrm{Re}_b = 114.06$. *The solid area fractions for the three systems are the same at* $f_a = 25\%$.

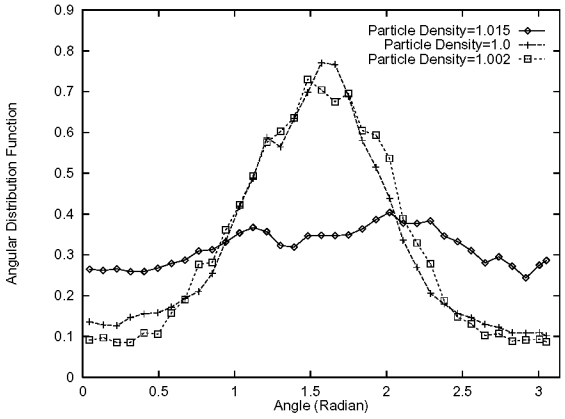

FIG. 16. *The averaged angular distribution across the channel for the same cases as in Fig. 15.*

the Segré-Silberberg phenomenon is clearly observed in the simulations. A single elliptic particle migrates to an equilibrium position between the walls and the centerline of channel due to the inertial lift associated with the curvature of velocity profile. The equilibrium position of the particle in the cross flow direction is independent of the initial position and orientation of the particle. At the equilibrium, an ellipse is much more likely to align its long end along the flow direction than along the cross flow direction, because the torque from the flow on the particle is weaker when the particle align its long axis with the flow. Our simulations demonstrate that the Segré-Silberberg effect also exists in a multi-particle system, and is responsible for driving the particles away from the centerline. Consequently, the particle volume fraction distribution across the channel has two maxima located at both side of the centerline and has one minimum at the centerline. The velocity profile has two shoulders corresponding to the maxima in the particle volume fraction distribution. As the total particle volume fraction increases, the maxima in the particle volume fraction distribution become wider and the minimum disappears gradually. In the mean time, the shoulders in the velocity profile become more and more prominent and the velocity profile becomes more and more blunt. It is clear that the Segré-Silberberg phenomenon in a single elliptic particle system is caused by the wall lubrication repulsion, an inertial lift due to shear slip, a lift due to rotation and a lift associated with velocity curvature. However, the Segré-Silberberg effect is greatly reduced as the total particle volume

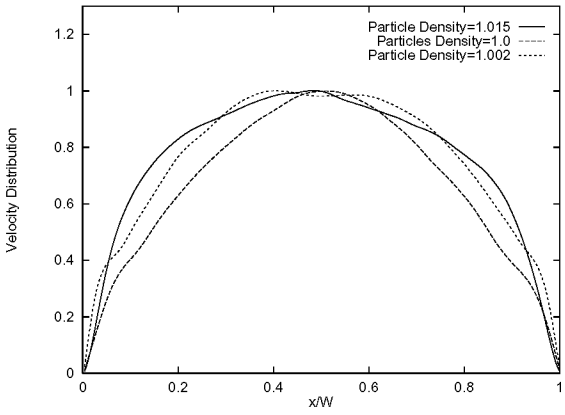

FIG. 17. *The averaged velocity distribution across the channel for the same cases as in Fig. 15. The profile is normalized by the maximum velocity of suspensions for each case.*

fraction increases, and virtually vanishes as the total particle volume fraction increases beyond 40%, because multi-particle interaction changes velocity profile and reduces rotational motion of the particles. Ellipses preferentially align its long axis along the flow direction for the values of the total particle volume fraction considered here.

Secondly, when the particle density is slightly heavier than the fluid, a single particle leads ahead the flow and moves to a position away from the channel centerline, because the inertial lift points to the wall. When the particle density is large enough, the particle moves back to the centerline. In this case, the slip velocity overshadows the effect of the velocity profile. The wall lubrication repulsive force becomes dominant and the particle motion is similar to sedimentation. The ellipse turns to the cross flow direction. The behavior of the two-way migration of the ellipse is the same as that found by Feng, Hu and Joseph [6, 7] and Huang, Feng and Joseph [10, 11] for a circular particle. This two-way migration behavior remains in a multi-particle system, *i.e.*, the particles slightly lighter than the fluid move away from the centerline, and the particles which are heavy enough move back to the centerline. The likelihood that the ellipses align their long axes with the flow direction is greatly reduced due to the sedimentation effect.

And finally, when the particle density is smaller than the fluid density, a particle lags behind the velocity of flow, the inertial lift and wall repulsion grow and push the particle to the centerline. As the density difference between the particle and the fluid (buoyancy) increases, the particle is concentrated at the centerline region. Oscillations about the centerline are observed in some cases. For multi-particle systems, the maxima in the particle volume fraction distribution across the channel increases, while both the angular distribution and the velocity profile become flat, as respectively shown in Figs. 14 and 16, due to buoyant forces and multi-particle interactions.

Acknowledgments. DWQ acknowledges the partial support from the donors of The Petroleum Research Fund, administered by the ACS, and the computing time awarded by National Computational Science Alliance, NERSC, and Pittsburgh Supercomputing Center.

REFERENCES

[1] C.K. AIDUN AND Y. LU, *Lattice Boltzmann simulation of solid suspensions with impermeable boundaries*, J. Stat. Phys., 81 (1995), pp. 49–61.

[2] C.K. Aidun, Y. Lu, and E. Ding, *Direct analysis of particulate suspensions with inertia using the discrete Boltzmann equation*, J. Fluid Mech., 373 (1998), pp. 287–311.

[3] H. Brenner, *Hydrodynamic resistance of particles at small Reynolds numbers*, Adv. Chem. Engng., 6 (1966), pp. 287.

[4] R.G. Cox and S.G. Mason, *Suspended particles in fluid flow through tubes*, Annu. Rev. Fluid Mech., 3 (1971), pp. 291.

[5] D. d'Humières, P. Lallemand, and U. Frisch, *Lattice gas model for 3D hydrodynamics*, Europhys. Lett., 2 (1986), pp. 291–297.

[6] J. Feng, H.H. Hu, and D.D. Joseph, *Direct simulation of initial value problems for the motion of solid bodies in a Newtonian fluid. Part 1. Sedimentation*, J. Fluid Mech., 261 (1994), pp. 95–134.

[7] ——*Direct simulation of initial value problems for the motion of solid bodies in a Newtonian fluid. Part 2. Couette and Poiseuille flows*, J. Fluid Mech., 277 (1994), pp. 271–301.

[8] F. Feuillebois, *Some theoretical results for motion of solid spherical particles in a viscous fluid*, in *Multiphase Science and Technology*, Vol. 4 (1989), ed. G.F. Hewitt *et al.*, pp. 583–789.

[9] X. He and L.-S. Luo, *A priori derivation of the lattice Boltzmann equation*, Phys. Rev. E, 55 (1997), pp. R6333–R6336.

[10] P. Huang, J. Feng, and D.D. Joseph, *The turning couples on an elliptic particle settling in a vertical channel*, J. Fluid Mech., 271 (1994), pp. 1–16.

[11] ——, *Direct simulation of the sedimentation of elliptic particles in Oldroyd-B fluids*, J. Fluid Mech., 362 (1998), pp. 297.

[12] D.D. Joseph, *Interrogations of Direct Numerical Simulation of Solid-Liquid Flows*, `http://www.aem.umn.edu/people/faculty/joseph/interrogation.html` (2001).

[13] D.L. Koch and A.J.C. Ladd, *Moderate Reynolds number flows through periodic and random arrays of aligned cylinders*, J. Fluid Mech., 349 (1997), pp. 31–66.

[14] A.J.C. Ladd, *Numerical simulations of particulate suspensions via a discretized Boltzmann equation. Part 1. Theoretical foundation*, J. Fluid Mech., 271 (1994), pp. 285–309.

[15] ——, *Numerical simulations of particulate suspensions via a discretized Boltzmann equation. Part 2. Numerical results*, J. Fluid Mech., 271 (1994), pp. 311–339.

[16] L.G. Leal, *Particle motion in a viscous fluid*, Annu. Rev. Fluid Mech., 12 (1980), pp. 435.

[17] L.-S. Luo, *Unified Theory of the lattice Boltzmann models for nonideal gases*, Phys. Rev. Lett., 81 (1998), pp. 1618–1621.

[18] G. McNamara and G. Zanetti, *Use of Boltzmann equation to simulate lattice-gas automata*, Phys. Rev. Lett., 61 (1988), pp. 2332–2335.

[19] D.W. Qi, *Non-spheric colloidal suspensions in three-dimensional space*, Int. J. Mod. Phys. C, 8 (1997), pp. 985–997.

[20] ——, *Computer simulation of coating suspensions*, in Proceedings of Tappi Advanced Coating Fundamental Symposium, May, 1997, Philadelphia, PA, pp. 201–211.

[21] ——, *Lattice Boltzmann Simulations of particles in Non-zero-Reynolds-number flows*, J. Fluid Mech., 385 (1999), pp. 41–62.

[22] ——, *Lattice Boltzmann simulations of fluidization of rectangular particles*, Int. J. Multiphase Fluid, 26 (2000), pp. 421–433.

[23] ——, *Simulations of fluidization of cylindrical multi-particles in a three-dimensional space*, Int. J. Multiphase Fluid, 27 (2001), pp. 107–118.

[24] D.W. Rebertus and K.M. Sando, *Molecular dynamic simulation of a fluid of hard spherocylinders*, J. Chem. Phys., 67 (1977), pp. 2585–2590.

[25] G. Segré and A. Silberbergi, *Radial Poiseuille flows of suspensions*, Nature, 189 (1961), pp. 209.

[26] ——, *Behavior of macroscopic rigid spheres in Poiseuille flow. Part 1.*, J. Fluid Mech., 14 (1962), pp. 115.

[27] S. Wolfram, *Cellular automaton fluids 1: Basic theory*, J. Stat. Phys., 45 (1986), pp. 471–526.

REPORT DOCUMENTATION PAGE

Form Approved
OMB No. 0704-0188

Public reporting burden for this collection of information is estimated to average 1 hour per response, including the time for reviewing instructions, searching existing data sources, gathering and maintaining the data needed, and completing and reviewing the collection of information. Send comments regarding this burden estimate or any other aspect of this collection of information, including suggestions for reducing this burden, to Washington Headquarters Services, Directorate for Information Operations and Reports, 1215 Jefferson Davis Highway, Suite 1204, Arlington, VA 22202-4302, and to the Office of Management and Budget, Paperwork Reduction Project (0704-0188), Washington, DC 20503.

1. AGENCY USE ONLY *(Leave blank)*	2. REPORT DATE	3. REPORT TYPE AND DATES COVERED
	July 2002	Contractor Report

4. TITLE AND SUBTITLE
LATERAL MIGRATION AND ROTATIONAL MOTION OF ELLIPTIC PARTICLES IN PLANAR POISEUILLE FLOW

5. FUNDING NUMBERS
C NAS1-97046
WU 505-90-52-01

6. AUTHOR(S)
Dewei Qi, Li-Shi Luo, Raja Aravamuthan, and William Strieder

7. PERFORMING ORGANIZATION NAME(S) AND ADDRESS(ES)
ICASE
Mail Stop 132C
NASA Langley Research Center
Hampton, VA 23681-2199

8. PERFORMING ORGANIZATION REPORT NUMBER
ICASE Report No. 2002-21

9. SPONSORING/MONITORING AGENCY NAME(S) AND ADDRESS(ES)
National Aeronautics and Space Administration
Langley Research Center
Hampton, VA 23681-2199

10. SPONSORING/MONITORING AGENCY REPORT NUMBER
NASA/CR-2002-211661
ICASE Report No. 2002-21

11. SUPPLEMENTARY NOTES
Langley Technical Monitor: Dennis M. Bushnell
Final Report
To appear in the Journal of Statistical Physics.

12a. DISTRIBUTION/AVAILABILITY STATEMENT
Unclassified–Unlimited
Subject Category 34
Distribution: Nonstandard
Availability: NASA-CASI (301) 621-0390

12b. DISTRIBUTION CODE

13. ABSTRACT *(Maximum 200 words)*
Simulations of elliptic particulate suspensions in the planar Poiseuille flow are performed by using the lattice Boltzmann equation. Effects of the multi-particle on the lateral migration and rotational motion of both neutrally and non-neutrally buoyant elliptic particles are investigated. Low and intermediate total particle volume fraction $f_a = 13\%$, 15%, and 40% are considered in this work.

14. SUBJECT TERMS
elliptic particulate suspensions in the planar Poiseuille flow, lateral migration, rotational motion, multi-particle interaction, the Segré and Silberberg effect, lattice Boltzmann simulation

15. NUMBER OF PAGES
19

16. PRICE CODE
A03

17. SECURITY CLASSIFICATION OF REPORT	18. SECURITY CLASSIFICATION OF THIS PAGE	19. SECURITY CLASSIFICATION OF ABSTRACT	20. LIMITATION OF ABSTRACT
Unclassified	Unclassified		